Enhancement in the diffusivity of Brownian spheroids in the presence of spheres

Vikki Anand Varma, Isha Malhotra, and Sujin B. Babu*
Out of Equilibrium Group, Department of Physics, Indian Institute of Technology Delhi, New Delhi 110016, India

(Received 8 November 2021; revised 30 May 2022; accepted 13 June 2022; published 14 July 2022)

In the present paper, we have extended the simulation technique Brownian cluster dynamics (BCD) to analyze the dynamics of the binary mixture of hard ellipsoids and spheres. The shape dependent diffusional properties have been incorporated into BCD using Perrin's factor and compared with analytical results of a one-component ellipsoidal system. We have investigated pathways to enhance the diffusivity of spheroids in the binary mixture by manipulating the phase behavior of the system through varying the fraction of spheres in the binary mixture. We show that at low volume fraction the spherical particles have a higher diffusion coefficient than the ellipsoids due to the higher friction coefficient. However, at a higher volume fraction, we show that the diffusion coefficient of the ellipsoids increases irrespective of the aspect ratio due to the anisotropic shape.

DOI: 10.1103/PhysRevE.106.014602

I. INTRODUCTION

Colloidal systems have been investigated for more than a century, as these systems can mimic atomistic phenomena and can also be tracked on a single particle scale because of their micrometer size. The spherical colloidal particles have been one of the most extensively studied systems both experimentally as well as theoretically. In these studies, the phenomena being investigated include transient clustering, jammed systems, crystal formation, etc. [1–8]. Recent experimental advancements have made it possible to synthesize colloids of different shapes [9–12]. Among these particles, the anisotropic colloidal particle has attracted a lot of interest [10,11,13–19]. These ellipsoidal particles display a rich variety of phases which include nematic phase, crystallization, smectic phase, etc. [20,21]. Recently, the dynamics of hard-core ellipsoidal particles has revealed two types of glass transition, repulsive glass in terms of translation [22] and orientational or liquid glass in terms of rotational jamming [13]. To simulate the liquid glass, the ellipsoidal particles have been simulated by introducing a rough wall in the system, to avoid isotropic-nematic transition.

In simulations, binary system containing hard spheroids have been studied extensively. Most of these works are focused on the study of phase behavior related to nematic ordering. These studies include binary systems of hard rods–spheroids [23] and spheres-plates [24]. The binary system of spheres and spheroids has also been studied [25], while considering the spheres as impurity. The binary system of spheres and spheroids with a combination of different shapes and sizes has been analyzed by using density functional theory [26] as well. In this paper, we have simulated a binary system of colloids with spheres and spheroids. We used Brownian cluster dynamics (BCD) to study the diffusivity of the binary colloidal system, both in the dilute and high concentration limit, up to the nematic phase.

To study the phase properties and dynamics of spheroids by simulation, a variety of techniques have been proposed which include molecular dynamics [21,27–29], Monte Carlo [17,30–32], Langevin dynamics [5,33] etc. Brownian cluster dynamics is a simulation technique, primarily developed to study the structure, kinetic, and dynamical properties of colloidal systems. BCD can be considered as a variant of the Monte Carlo method but with the added advantage of being able to predict the kinetics and dynamics of the system [34]. The rigidity of the bond formed between particles in BCD can be controlled very easily for equilibrium configuration [35]. Using the BCD technique both reversible and irreversible aggregation was studied on a lattice [36,37], later extending the technique to off-lattice spherical particles with an isotropic square-well potential, for both one-component [7,35,38–40] and binary colloidal systems [41,42]. It was already shown that the structure, kinetics, and dynamics of BCD with the Rouse model agree with event-driven Brownian dynamics (EDBD) for the case of square-well potential [34]. Recently, BCD was modified to simulate spherical patchy particles [43–46] using the Kern-Frenkel potential [30]. The method was validated by showing the correct static and dynamic properties for a single polymer chain [43]. The aggregation of the lysozyme protein was mimicked using spherical particles with two patches having irreversible bonds with an overlapping isotropic reversible square-well potential [44,45].

BCD technique is composed of two steps, the cluster construction step and the movement step. In the present paper, we are exploring only the dynamics of the athermal mixture of hard ellipsoid and spherical particles. Within the given framework of BCD, we study the dynamics of the system by scaling the physical time, as equal to the time taken by a particle to diffuse a length of its own diameter. In BCD we do not solve the equation of motion, which can be computationally expensive for the particles like spheroids. The particles are moved in a random direction with a fixed translational and rotational step length. By calibrating step length, we can scale large physical time for the same number of simulation

*sujin@physics.iitd.ac.in

times. In this way, we can study the kinetics of the system for a longer time as it will be computationally less expensive. In the present paper, we have extended the BCD technique to include hard spheroids. We mimic the diffusive motion of a single spheroid by implementing the friction coefficient in terms of translational and rotational step length. We have considered the shape dependent friction of spheroids as given by Perrin *et al.* [47] for the stick boundary condition. In the binary mixture of spheres and spheroids, we found Perrin's friction factor playing an important role behind the observed enhancement in the translational and rotational diffusivities of the spheroids, with an increasing fraction of spheres. As we increase the fraction of spheres in the binary mixture keeping the same volume fraction, the nematic phase vanishes which is also observed in the case of rod-sphere mixture [23]. It was also observed that the enhancement of diffusivity of the spheroid is due to the anisotropy of the spheroids.

The paper is arranged as follows: in Sec. II we give a detailed explanation regarding the inclusion of asymmetrical particles into the simulation technique Brownian cluster dynamics. We also explain how we incorporated the friction equation derived by Perrin *et al.* [47] as well as the way we reformulated the definition of time in BCD. In Sec. III we have discussed the effect of step size to mimic Brownian dynamics, as well as compared the result of one ellipsoidal particles to the analytical equation derived by Perrin *et al.* for the single particle diffusion. The shape of the isodiffusivity lines of BCD and EDBD shows a similar trend both for translational and rotational diffusion. We have shown that the translational diffusion of a binary system consisting of sphere and ellipsoidal particles both prolate and oblate depends on the aspect ratio, and the rotational diffusion depends on the nematic transition. We have also reported a nematic to isotropic transition for different fractions of the sphere as a function of volume fraction in a binary system. This is followed by the conclusion in Sec. IV.

II. SIMULATION METHOD

We have modified BCD to incorporate spheroid (prolate and oblate) particles. The spheroids are defined by the aspect ratio $p = a/b$, where a and b are the lengths of the semimajor (symmetry axis) and semiminor (perpendicular to the symmetry axis) axes respectively. We represent an ellipsoid of revolution (ER) with the orientation of a unit vector $\hat{n}$ along the symmetry axis and the position vector of the center of mass. In the present paper, we have considered $N = 600$ particles in a cubic simulation box of size L, with periodic boundary condition [48]. The ellipsoids with different p considered in the present paper have a volume equal to the volume of a sphere with diameter $d = 1$ such that $d = (ab^2)^{1/3}$. The corresponding volume fraction is defined as $\phi = N\frac{\pi d^3}{6L^3}$, where N is the number of spheroids and L is the length of the simulation box.

We create a random distribution of both the position and orientation of the ellipsoidal particle inside the simulation box. We then randomly select $2N$ ER for the movement step. The selected particle undergoes either a translational or rotational displacement in a random direction, with a probability of half. This ensures that the translational and rotational motion of ellipsoids occurs in an uncorrelated manner [34,43]. The rotational and translational displacement of the ellipsoids occurs in a random direction with a predefined step length S_T and S_R, respectively. Each movement step is followed by an overlap condition to check the overlap of the hard-core ellipsoidal particles. The movement step is only accepted if there is no overlap with other ellipsoidal particles.

For calculating the overlap condition of the ellipsoidal particles, we define a rectangular box enclosing the ER, with length and breadth twice those of the semimajor and semiminor axis respectively. If the oriented bounding boxes [49] of two adjacent ellipsoids overlap, then we employ the method of the ellipsoidal contact function [50] to verify the overlap of the particles. After we have attempted to translate or rotate the $2N$ particles, we increment the simulation time $t_{\rm sim}$ by one unit, which is the number of times we have attempted to translate and rotate all the particles in the system.

To achieve a particular volume fraction, ϕ with random initial condition, we distribute 600 particles in a large simulation box or in other words at very low ϕ. We gradually reduce the size of the simulation box from all sides gradually [26], until the desired ϕ is achieved. After each compression step, we relax the system for 10^4 simulation time before performing the next compression procedure. After compressing the system, we relax it for another 2×10^6 simulation time, which is the starting configuration for all the results reported in the present paper.

Dynamics

In BCD the center of mass of the particle undergoes a translation with constant step size S_T in a random direction [34]. When S_T is small, the random walk of the center of mass of a sphere can be approximated to a diffusion problem [51]. For a single sphere, the relation between the physical time $t_{\rm phy}$ and the simulation time $t_{\rm sim}$ is given by

$$\frac{\langle R^2\rangle}{d^2} = t_{\rm sim}\frac{{S_T}^2}{d^2} = 6D_T^{\circ}\frac{t_{\rm phy}}{t_0} \tag{1}$$

where $\langle R^2\rangle$ is the mean square displacement (MSD) of the center of mass of the sphere. t_0 is defined as the time taken by a single sphere to travel its own diameter d, such that $D_T^{\circ} = 1/6$ which is the translational diffusion coefficient of a single sphere. In the present paper the simulation time is defined as $\frac{t_{\rm phy}}{t_0} = t_{\rm sim}\frac{{S_T}^2}{d^2}$ as we have considered all the ellipsoids to have a volume equal to a sphere with $d = 1$.

The ellipsoid will also undergo a random rotation along the symmetry axis. Along the other two perpendicular axes to the symmetry axis, no rotation is undertaken as it is symmetric. The random rotation of the tip of the unit vector $\hat{n}$ along the symmetry axis of ER will perform a two dimensional random walk, on the surface of a sphere with a step size S_R, similar to rotation done for spherical patches [43,44]. When the step size is small, it will undergo rotational diffusion with a diffusion coefficient D_R. In the limit $D_R t \ll 1$,

$$\langle(\hat{\mathbf{n}}(t) - \hat{\mathbf{n}}(0))^2\rangle = t_{\rm sim}\frac{{S_R}^2}{d^2} = 4D_R^{\circ}\frac{t_{\rm phy}}{t_0} \tag{2}$$

where D_R° is the rotational diffusivity of the vector and we can show that $\sqrt{2}S_T = S_R$ [43].

For a spherical particle we know from the Stokes-Einstein relation for diffusion that D_T and D_R are related to the friction coefficient as [52]

$$D_T = \frac{k_B T}{\gamma}, \tag{3a}$$

$$D_R = \frac{k_B T}{\gamma_\theta} \tag{3b}$$

where k_B is the Boltzmann constant and T is the temperature. γ and γ_θ are the friction coefficients for the translational and rotational diffusion, respectively, given by

$$\gamma = 6\pi\eta\frac{d}{2}, \tag{4a}$$

$$\gamma_\theta = 6\eta V^o \tag{4b}$$

where η is the viscosity of the solvent and V° is the volume of the particle.

For the asymmetric ellipsoidal particle, the diffusion coefficient D_T is resolved along the parallel and perpendicular plane of the symmetry axis as

$$D_T = \tfrac{2}{3}D_T^{\parallel} + \tfrac{1}{3}D_T^{\perp} \tag{5}$$

where $D_T^{\perp}$ is the diffusion coefficient in the perpendicular direction of the symmetry axis and $D_T^{\parallel}$ is the diffusion coefficient parallel to the symmetry axis.

The change in D_T and D_R for an ellipsoidal particle compared to a spherical particle can be expressed in terms of the friction coefficient γ and γ_θ given by [53]

$$\gamma^{\perp or\parallel} = 6\pi\eta b G_T^{\perp or\parallel}, \tag{6a}$$

$$\gamma_\theta = \eta V^o G_\theta \tag{6b}$$

where b is the length of the semiminor axis and G is the Perrin friction factor [47,54]. G measures the deviation in friction coefficient when the particle deviates from spherical to ellipsoidal shape. G_θ gives the deviation in the rotational friction coefficient. $G_T^{\parallel}$ and $G_T^{\perp}$ denote the translational friction coefficients along the parallel and perpendicular direction of the symmetry axis respectively. For the stick boundary condition at the surface of spheroids, the factor G [47,55] for the prolate case $p > 1$ is given as

$$G_T^{\parallel} = \frac{4}{3}\left[\frac{p}{(1-p^2)} + \frac{2p^2-1}{(p^2-1)^{3/2}}\ln(p+\sqrt{p^2-1})\right]^{-1}, \tag{7a}$$

$$G_T^{\perp} = \frac{8}{3}\left[\frac{p}{(p^2-1)} + \frac{2p^2-3}{(p^2-1)^{3/2}}\ln(p+\sqrt{p^2-1})\right]^{-1}, \tag{7b}$$

$$G_\theta = \frac{2}{3}\frac{(p^4-1)}{p}\left[\frac{(2p^2-1)}{\sqrt{p^2-1}}\ln(p+\sqrt{p^2-1}) - p\right]^{-1}. \tag{7c}$$

For the oblate case, $p < 1$,

$$G_T^{\parallel} = \frac{4}{3}\left[\frac{p}{(1-p^2)} + \frac{1-2p^2}{(1-p^2)^{3/2}}\arccos(p)\right]^{-1}, \tag{8a}$$

$$G_T^{\perp} = \frac{8}{3}\left[\frac{p}{(p^2-1)} + \frac{3-2p^2}{(1-p^2)^{3/2}}\arccos(p)\right]^{-1}, \tag{8b}$$

$$G_\theta = \frac{2}{3}\frac{(p^4-1)}{p}\left[\frac{(2p^2-1)}{\sqrt{1-p^2}}\arccos(p) - p\right]^{-1}. \tag{8c}$$

The parameter $G \to 1$, as the aspect ratio $p \to 1$, which corresponds to a sphere.

We have kept S_T constant in the present paper. To incorporate the effect of anisotropic diffusion, we have introduced two different step sizes, along the parallel direction $S_T^{\parallel}$ and along the perpendicular direction $S_T^{\perp}$ of the symmetry axis. The diffusion of ER along the direction parallel to the symmetry axis was compared with that of a sphere with the same volume; using Eq. (1), it can be shown that $D_T^{\parallel}/D_T^{\circ} = (S_T^{\parallel})^2/S_T^2$. Combining Eqs. (3), (4), and (6) the relation between the transitional and rotational step size of the ER compared to a sphere of the same volume can be calculated by

$$\frac{S_T^{\perp,\parallel}}{S_T} = \sqrt{\frac{d}{2bG_T^{\perp or\parallel}}}, \tag{9a}$$

$$\frac{S_R^e}{S_T} = \sqrt{\frac{2}{G_\theta}}. \tag{9b}$$

In the simulation, we fixed the step size $S_T^2 = \frac{2}{3}(S_T^{\parallel})^2 + \frac{1}{3}(S_T^{\perp})^2$; similarly the step size for rotational diffusion is calculated from Eq. (9b).

III. RESULTS

A. Dynamics of one-component spheroids

In BCD, step size plays a major role in deciding the correct dynamics of the system. The step size has to be small to attain the correct diffusion coefficient. Large step sizes lead to a lot of rejection in the movement step due to the overlap condition, which leads to the diffusion coefficient being smaller than the expected value. To understand the effect of step size S_T we have calculated the long-time diffusion coefficient $D_T/D_T^{\circ} = \frac{\langle R^2\rangle/d^2}{t_{\rm phy}/t_0}$ for the prolate ellipsoidal particle in $\phi = 0.5$ and $p = 4$, with respect to step size as shown in Fig. 1. The MSD is defined as $\langle R^2\rangle = \frac{1}{N}\sum_{i=1}^{N}[r_i(t) - r_i(0)]^2$ where r_i is the position of the center of mass of the ellipsoidal particle as a function of time. In Fig. 1 we observe that D_T/D_T° increases with reducing step size and converges to 0.18. The distance between the ellipsoids in the equilibrium configuration for $\phi = 0.5$ is very small. The step size we choose should be less than the nearest neighbor distance between particles for a particular ϕ. For step sizes larger than the interparticle distance there will be more rejections in the movement step due to the collision with the nearby ellipsoidal particle. Thus the center of mass of many particles will not be able to diffuse, leading to D_T/D_T° smaller than the expected value. To avoid this problem, if we continue to reduce S_T, the physical time over which we can probe our system will also reduce according to Eq. (1). As a compromise, we have chosen a step size the diffusion coefficient of which is accurate within 10% of the real value, where the step size $S_T = 0.005$ is kept constant for all the systems reported in the present paper irrespective of the aspect ratio. We observe that the long-time diffusion coefficients $D_T^{\parallel}/D_T^{\circ}$ and $D_T^{\perp}/D_T^{\circ}$ follow the same trend as the center of mass diffusion coefficient for the oblate and prolate particles.

In Fig. 2, we have plotted the mean square displacement of the prolate ER as a function of time, at $\phi = 0.5$, aspect

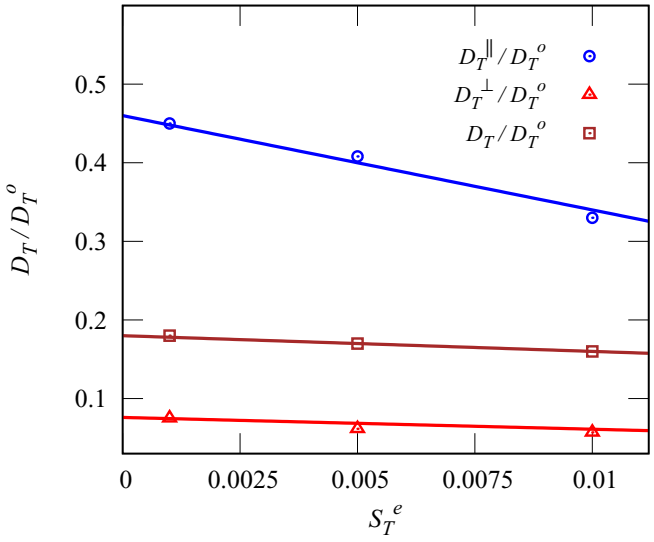

FIG. 1. The effect of step size (S_T) of the center of mass of ER with $D_T^{\parallel}/D_T^{o}$(circles), $D_T^{\perp}/D_T^{o}$ (triangles), and the resultant D_T/D_T^{o} (squares) shown for ER with $p = 4.0$ at $\phi = 0.5$. The solid lines are fit to the points. The points can be seen converging to a particular value, given by $D_T^{\parallel}/D_T^{o} \approx 0.46$, $D_T^{\perp}/D_T^{o} \approx 0.075$, and $D_T^{e}/D_T^{o} \approx 0.18$.

ratio $p = 4$, and step size $S_T/d = 0.005$. We also plotted the MSD along the parallel $\langle R_{\parallel}^2 \rangle$ and $\langle R_{\perp}^2 \rangle$ perpendicular to the symmetry axis of the ellipsoids as a function of time. We know that in the case of molecular dynamic simulation short-time dynamics always leads to ballistic motion, but in the case of BCD even the short-time dynamics undergoes Brownian motion. This can be observed in Fig. 2, as the slope of MSD remains unity even for short-time diffusion. After a long time $t_{\rm phy}/t_0 > 8$, the MSD again attains a slope of unity but with a slightly smaller diffusion coefficient due to the hindrance of the other ellipsoidal particles, as the volume fraction is finite. We also observe that the MSD along the perpendicular direction to the symmetry axis diffuses slower than the parallel

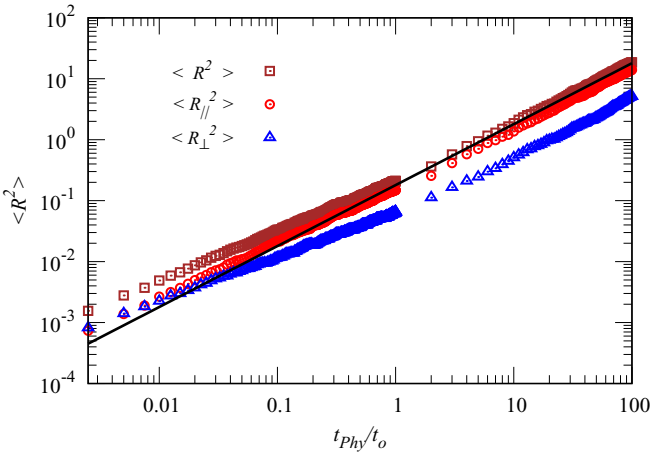

FIG. 2. The MSD of the center of mass of the ER $\langle R^2 \rangle/d^2$ (square) is plotted as a function of $t_{\rm phy}/t_o$ calculated with $S_T = 0.005$ for $p = 4$ and at $\phi = 0.50$. The MSD is resolved into the parallel (circle) and perpendicular (red points) direction of the director. They converge to a slope of unity as shown by the solid lines.

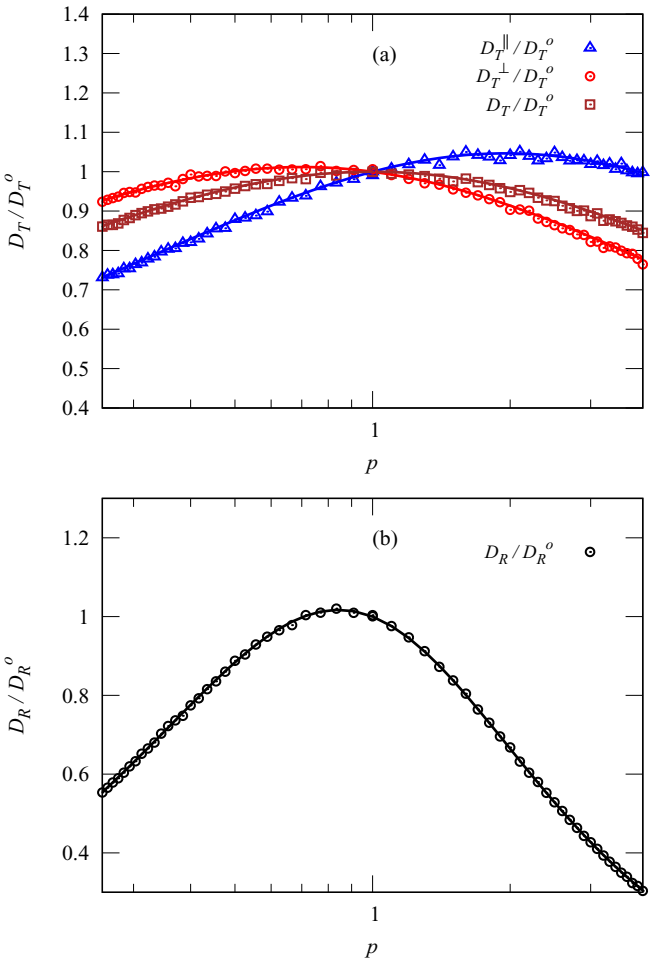

FIG. 3. (a) $D_T^{\parallel}/D_T^{o}$ (circles), $D_T^{\perp}/D_T^{o}$ (triangle), and D_T/D_T^{o} (square) shown for the different values of p at $\phi = 0.002$. Solid lines represent the analytical diffusion coefficient calculated for the single particle with a constant volume of $\pi/6$ for different values of p. (b) The change in D_R/D_R^{o} with respect to p shown for the present paper (circle) and analytical calculation from the Perrin factor shown with solid lines.

direction, as the friction coefficient along the perpendicular direction is larger compared to the parallel direction.

We know that the diffusion of the ellipsoidal particle should depend on the geometry of the particle. At lower volume fraction $\phi = 0.002$, the number of collisions with neighboring particles will be minimal and the ellipsoidal particle will diffuse like a single noninteracting ER. In Fig. 3(a) we have plotted $D_T^{\parallel}/D_T^{\circ}$, $D_T^{\perp}/D_T^{\circ}$ and D_T/D_T° for $\phi = 0.002$, as a function of the aspect ratio p, as obtained from the simulation. It is compared with the analytical equation of the single ER diffusion coefficient calculated using Eqs. (3), (6), and (7), and we observe good agreement with the simulation result for infinite dilution. We also observe that D_T/D_T° decreases with increasing shape anisotropy of the ER, as the friction coefficients for prolate and oblate particles increase along the perpendicular and parallel direction according to Eq. (7). In Fig. 3(b) we have plotted the rotational diffusion coefficient for both prolate and oblate ellipsoidal particles. We calculate the mean squared angular displacement of the ellipsoidal particle $\langle \theta_1^2 \rangle$, where θ_1 is defined as the angle formed by

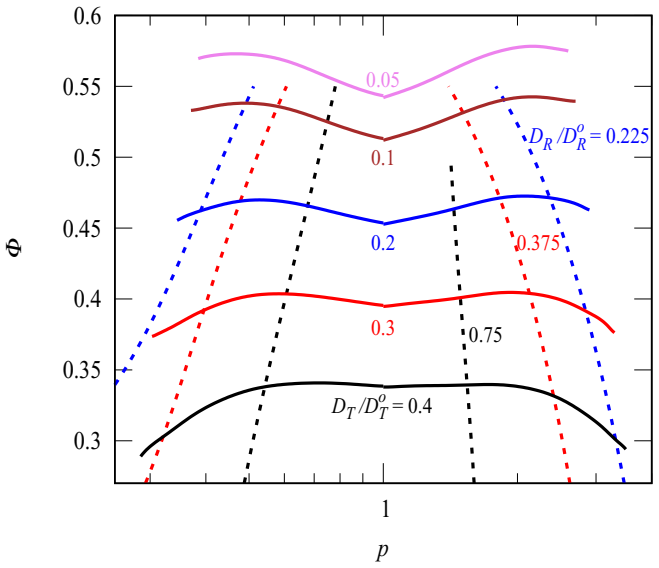

FIG. 4. Isodiffusivity lines shown for different ϕ as a function of the aspect ratio p, where the solid lines and dotted line represent translational and rotational diffusion respectively. The diffusion coefficients are as indicated in the figure.

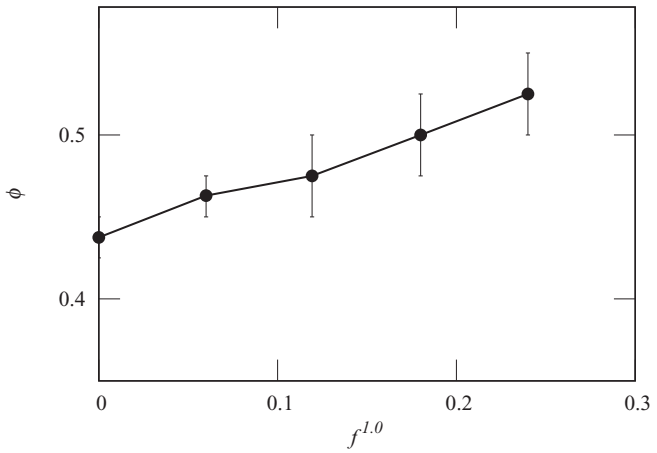

FIG. 5. Variation in the isotropic-nematic coexistence density ϕ with respect to the fraction of sphere $f^{1.0}$, present in the binary mixture of sphere and prolate $p = 4$ system, where upper and lower ticks on the error bar indicate nematic and isotropic phase, respectively, confirmed by nematic order-parameter calculation in the simulation.

the symmetry axis of the ER between a movement step. The movement of the symmetry axis being two dimensional, we have defined the rotational diffusion as $D_R/D_R^\circ = \frac{\langle\theta_1^2\rangle}{t_{\rm phy}/t_\circ}$. In Fig. 3(b) we observe that rotational diffusion is asymmetric for prolate and oblate ER. The simulation results agree perfectly with the theoretical curve given by Eqs. (6)–(8) for an infinitely dilute system.

In Fig. 4 we have plotted the isodiffusivity lines for the both translational and rotational components of the ellipsoidal particles. We observed a similar trend as reported by De Michele *et al.* [28] for the diffusion coefficient. The swallowlike shape of the translational isodiffusivity line as reported by the event-driven Brownian dynamic method for the fluid of spheroids is reproduced by the BCD technique as well. The value of the diffusion coefficient will not match EDBD, as in BCD we use Perrin's factor to mimic the dynamics, except at $p = 1$, where EDBD and BCD agree perfectly, as already demonstrated by Babu *et al.* [34], and reproduced in the present paper. The rotational diffusion isodiffusivity line shows that D_R/D_R° reduces when the aspect ratio or ϕ increases, as reported by Tang *et al.* [56]. The rotational diffusion coefficient of BCD also follows the isotropic-nematic transition, as shown for the EDBD method [28].

B. Isotropic-nematic transition in the spheroids-spheres binary mixture

We have already shown that using the BCD method, the dynamics of one-component hard spheroids can be modeled. We now advance the study to binary systems, consisting of a combination of prolate-sphere and oblate-sphere systems. We define the number fraction of one of the components of the binary system as $f^p = n_p/N$ where n_p is the number of spheroids present in the system corresponding to a particular aspect ratio p. The volume fraction of the binary system having N particles, which includes both spheres and spheroids, is calculated as $N/L^3\pi/6$, since the volume of the individual particles is kept equal to a sphere of diameter unity.

We calculate the nematic order parameter S for the binary mixture. S is the largest eigenvalue of the tensor Q defined by

$$Q_{\alpha,\beta} = \frac{3}{2}\frac{1}{N}\sum_i \langle (n_\alpha)_i (n_\beta)_i \rangle - \frac{1}{2}\delta_{\alpha,\beta} \tag{10}$$

where $(n_\alpha)_i(n_\beta)_i \in (n_x)_i, (n_y)_i, (n_z)_i$ with $(n_\alpha)_i$ the component of the orientation of the symmetry axis of ER. Here $S = 0$ means the purely isotropic phase, while $S > 0.3$ represents the nematic phase [28]. In Fig. 5 we have plotted the critical value of ϕ, where the transition from the isotropic to nematic phase is observed as a function of the fraction of the sphere in the binary mixture when $p = 4$ for the prolate particles. For an ellipsoidal system of one component with $p = 4$, we observe that the isotropic nematic transition occurs at $\phi \sim 0.43$. The isotropic nematic transition is shown to be weakly first order in nature [57]. As shown by Eppenga and Frenkel the minimum number of particles in the nematic phase should be above 400 to match with the theoretical calculation [58], which we have confirmed in the present paper. They have shown that the system is in the nematic phase when $S > 0.3$. In the present paper, we have simulated 20 independent configurations for each ϕ and f^p. When all the configurations give $S > 0.4$ we identify the system to be in the nematic phase. Similarly, when all the 20 configurations have $S < 0.2$, we identify the system to be in the isotropic phase. The upper and lower ticks on the error bar of the phase diagram in Fig. 5 correspond to these two volume fractions and the point is an average of the volume fractions, for a particular $f^{1.0}$. For example at $f^{1.0} = 0.12$, we found that $S > 0.4$ for $\phi \geqslant 0.5$ and $S < 0.2$ for $\phi \leqslant 0.45$. In the phase diagram we have shown this point at $\phi = 0.475$ with an error bar of ± 0.025. As we increase the volume fraction of the spheres, we observe that the isotropic nematic transition is stable at higher fractions of the sphere. It has already been shown analytically that the glass transition for one-component spheres and ellipsoids with

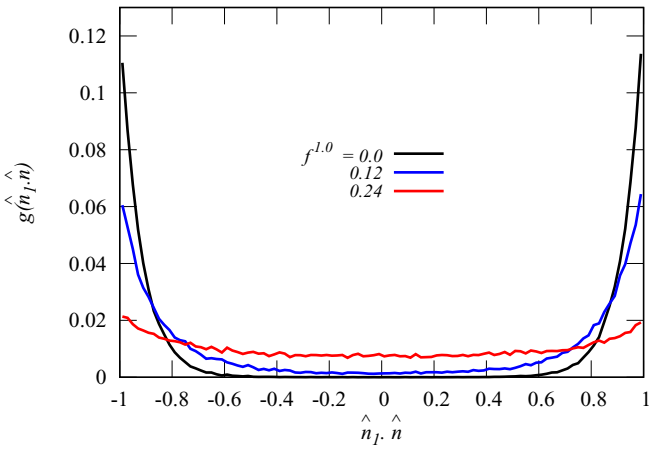

FIG. 6. $g(\hat{n}_I \cdot \hat{n})$ shown as a function of $\hat{n}_I \cdot \hat{n}$, which is the cosine of the angle made by the director with the symmetry axis of the prolate ellipsoids $p = 4$ at different fractions of spheres as mentioned in the figure.

$p = 4$ is around $\phi \sim 0.57$ [22]. So we have restricted this study up to a volume fraction of 0.55 as the main focus is on the diffusional properties of both spheres and ellipsoids.

In order to show the effect of spheres over the alignment of spheroids observed for the one-component prolate system, we have calculated the angular distribution $g(\hat{n}_I \cdot \hat{n})$, with respect to the nematic director $\hat{n}_I$ where $\hat{n}$ is the unit vector along the symmetry axes of the ellipsoids at equilibrium. In Fig. 6, we have plotted $g(\hat{n}_I \cdot \hat{n})$ of the ellipsoids in the binary mixture of prolate $p = 4.0$ and the sphere system at $\phi = 0.5$, for different fractions of spheres. In the nematic phase, the symmetry axis of the ellipsoids is either parallel or antiparallel to the director. The two peaks observed for $f^{1.0} = 0.0$ at $\hat{n}_I \cdot \hat{n} = 1$ and -1, indicating the presence of a high degree of alignment in the one-component system of spheroids as also confirmed by the calculation of the orientational order parameter. When the sphere fraction is 0.12 we observe that the fraction of aligned particles steadily decreases, although we have a nematic phase as confirmed by the S parameter calculation (see Fig. 5). When the fraction of spheres is further increased, we observe a curve where almost all the angles have a finite and near equal probability compared to the other fractions. This signifies an almost isotropic distribution of spheroids when the fraction is $\approx$0.24.

In order to understand the local ordering of the ellipsoidal system, we have calculated $g_{P_2}(r)$ and $g_2(r)$ defined as

$$g_{P_2}(r) = \left\langle \tfrac{1}{2}(3\cos^2\theta_r - 1) \right\rangle, \tag{11}$$

$$g_2(r) = \langle \cos(2\theta_r) \rangle \tag{12}$$

where θ_r is the angle between the symmetry axes of two ERs at a distance of r from the center of mass of the ER particle (see Fig. 7). For the nematic phase, we know that $g_{P_2}(r)$ will not decay to zero as can be observed for the case of one component $f^{1.0} = 0$ and 0.12. The orientational order for the one-component system can be clearly seen in a typical snapshot of the system at equilibrium in Fig. 8. The bounding box shown in Fig. 8(a) shows the area over which we are able to observe the nematic phase consistent with the $g_{P_2}(r)$ calculation of the one-component ellipsoidal system as shown in Fig. 7. In the binary system when $f^{1.0} = 0.12$ we observe that $g_{P_2}(r)$ relaxes to a constant value, consistent with the phase calculation, while $g_2(r)$ relaxes faster as it only explores the local order between ellipsoidal particles. In $g_2(r)$ calculation at $f^{1.0} = 0.12$ we observe local order up to a distance of $<2d$, as shown in the inset of Fig. 7 [also see Fig. 8(b)]. When the fraction is further increased to $f^{1.0} = 0.27$ the ordering decays much faster and confined to the distance smaller than the value $0.9d$ for both $g_{P_2}(r)$ and $g_2(r)$ calculation. This can be observed in the bounding box in Fig. 8(c), where the nematic order around the spheres is destroyed. Thus, we have confirmed that in a binary mixture of sphere-prolate systems, only local order is observed depending on the fraction of spherical particles present in a particular volume fraction.

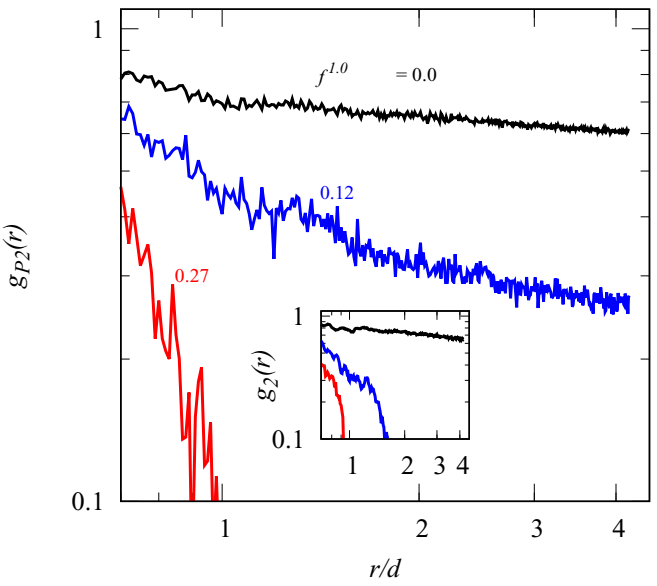

FIG. 7. $g_{P_2}(r)$ shown as a function of the distance r/d for a binary system of spheres and prolate $p = 4.0$, at $\phi = 0.50$, with a fraction of the sphere as indicated in the figure. The inset shows the calculation of $g_2(r)$ for the same configuration as indicated in the figure.

C. Dynamics in the two-component system of the spheroid-sphere

Figure 9 shows D_T/D_T° which is the diffusion coefficient of only one species of particle, spheres, or spheroids, in the

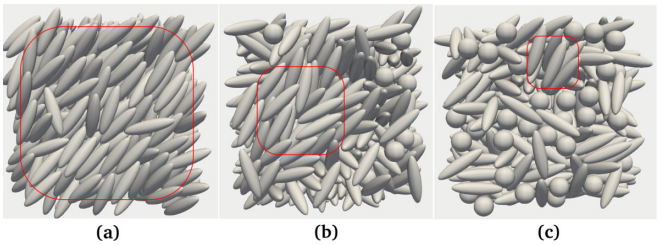

FIG. 8. Snapshot of the binary spheroidal-sphere system with an increasing fraction of the spherical particle from left to right for $\phi = 0.5$, $p = 4.0$ and at (a) $f^{1.0} = 0.0$, (b) $f^{1.0} = 0.12$, (c) $f^{1.0} = 0.27$. The ordered reason (the bounding box) can be seen decreasing with increasing the number of spheres in the system.

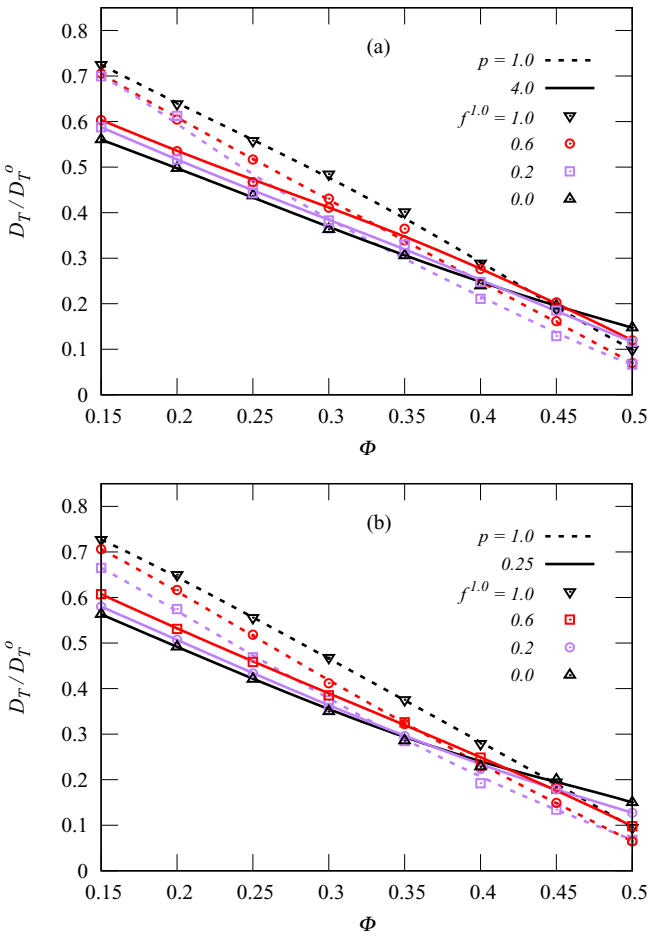

FIG. 9. (a) D_T/D_T^o shown for the binary system containing particles with sphere $p = 1.0$ and prolate $p = 4.0$. The solid symbols represent a guide to the eye representing the diffusion coefficient of only the prolate particles in the binary mixture. The short dashed line represents the diffusion coefficients of only the spherical particles. The fraction of spherical particles is as indicated in the figure. (b) D_T/D_T^o is plotted for an oblate $p = 0.25$ and sphere mixture. The lines which are a guide to the eye are diffusion coefficients for $p = 0.25$ (solid) and for spheres (short dash) for the fraction of sphere indicated in the figure.

binary system as a function of ϕ. In the binary mixture we have studied two combinations, one with spheres and the ER with $p = 4$ [see Fig. 9(a)] and one with spheres and ERs $p = 0.25$ [see Fig. 9(b)]. For the spherical one-component system $f^{1.0} = 1$, we observe that the diffusion coefficient of the sphere goes down monotonically [34]. For the oblate and prolate system of one component ($f^{1.0} = 0$) the diffusion coefficient for a low volume fraction is always smaller than the spherical system, which can also be observed in Fig. 3 for an infinitely dilute system. The diffusion coefficient of the spheroidal system goes down as we increase the volume fraction to $\phi < 0.35$ similar to the case of a hard sphere system. For $\phi > 0.35$ we observe that the slope of the diffusion curve of a one-component ellipsoidal particle increases and crosses the one-component spherical system. For the ellipsoidal system of one component, a nematic transition is expected for aspect ratio 4 [59–61], which is reproduced by the BCD technique. We observe that for $\phi > 0.43$ the translational diffusion coefficient of the one-component ellipsoidal system becomes higher than the spherical system. This effect has already been shown in the case of short-time diffusion coefficient for monomeric rods simulated with hydrodynamic interaction [10,19].

For the binary mixture with $f^{1.0} = 0.2$, we observe that D_T/D_T° of only the spheres in the mixture decreases compared to the case of one component $f^{1.0} = 1$, due to the presence of ER. For very low ϕ we observe that diffusion is controlled by the friction coefficient, and hence the sphere diffuses faster than ellipsoids. An interesting phenomenon we observe is that the diffusion coefficient of the ellipsoids increases in the presence of spherical particles for higher volume fraction compared to the one-component system of spheres having the same volume fraction. With increasing volume fraction of the binary system, the volume available to the center of mass of both spheres and ellipsoidal particle to diffuse decreases. As the number of spheres increases, the channels of free space available for the ellipsoidal particle to diffuse become narrower. When the average channel width of the free space becomes comparable to the diameter of the sphere, we observe that the diffusion coefficient of the spheres decreases dramatically in the binary system. For the ellipsoidal particles, as the semiminor axis is smaller than the radius of the sphere, it can squeeze through the channel, which is forbidden for the spheres due to the excluded volume of the binary mixture. As we increase the fraction of spherical particles to $f^{1.0} = 0.6$, we observe that the diffusion coefficient of the spherical particle in the binary mixture is lower compared to the diffusion coefficient at $f^{1.0} = 0.2$. When the fraction of spheres increases for the same volume fraction, the accessible volume becomes smaller for the isotropic spheres compared to that of the anisotropic particle. For the anisotropic particle, there is a competition between the friction coefficient, which reduces the diffusion coefficient compared to the sphere, and exploration of the more accessible volume due to the anisotropy of the ellipsoidal particles. For the fraction $f^{1.0} = 0.2$ the friction coefficient effect wins $\phi < 0.3$, as the accessible volume available for the binary mixture is large and thus the sphere diffuses faster. For $\phi > 0.3$ the ellipsoidal particle can squeeze through the free space channels created as the length of the minor axis is smaller than the radius of the sphere. For the case of oblate particles, we also observe a similar trend as for the case of prolate ellipsoidal particles. For the prolate case the crossover for $f^{1.0} = 0.2$ happens at a lower volume fraction $\phi \sim 0.3$ compared to the case of $f^{1.0} = 0.6$ where it happens at $\phi \sim 0.35$. In the oblate case, the crossover with the diffusion coefficient of the spherical particle occurs at a slightly higher volume fraction. For $\phi > 0.45$, in the binary mixture, the ellipsoidal particles see a decrease in D_T/D_T° in the presence of spheres, compared to the one-component ellipsoid case. The trend is opposite, as observed in the low ϕ regime, where diffusion is enhanced in the presence of spheres. At a higher volume fraction, the accessible volume available to the mixture will be smaller, as the average width of the free space channel will become comparable to the semiminor axis, and thus the ellipsoidal particles will slow down. In the case of one component, ellipsoidal particles, it undergoes nematic transition.

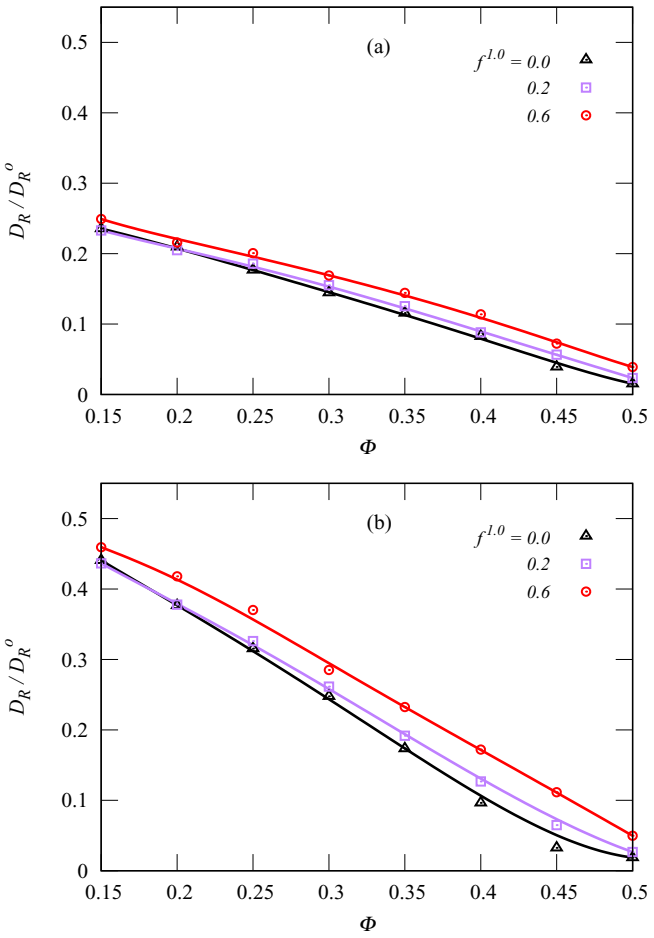

FIG. 10. (a) D_R/D_R^o shown for the binary system containing both sphere and prolate $p = 4$ particles at different ϕ. The fraction of the sphere is as given in the figure. The solid lines are guides to the eye. (b) $D_R^{0.25}/D_R^o$ is shown for the binary system containing both sphere and oblate $p = 0.25$ particles at different ϕ. The fraction of the sphere is as shown in the figure and solid lines are guides to the eye.

The isotropic nematic transition effect is clearly observed in the case of the rotational diffusion coefficient for the mixture with aspect ratio 4 and 1. In Fig. 10 we have plotted the D_R/D_R° as a function of volume fraction for $f^{1.0} = 0$, 0.2, and 0.6 for prolate [see Fig. 10(a)] and oblate [see Fig. 10(b)] binary systems. The $f^{1.0} = 0$ ellipsoidal system has a minimum rotational diffusion, which is expected as we observe the isotropic nematic transition for $\phi > 0.43$. For the case of $f^{1.0} = 0.2$, the rotational diffusion coefficient increases slightly compared to the case of one component. We also observe that the diffusion coefficient for $f^{1.0} = 0.2$ tends towards the one-component case for $\phi \geqslant 0.5$, as expected for higher volume fraction as the volume available for the ellipsoidal particle decreases. When the fraction $f^{1.0} = 0.6$, for the prolate and oblate ER in the binary mixture, we observe that the rotational diffusion coefficient is higher than for the system of one component. The reason could be that structurally there is a change in the system compared to the $f^{1.0} = 0$ case, and it may be the absence of isotropic nematic transition. Note that the glass transition for the one-component ellipsoidal and spherical particles is reported at a volume fraction greater than 0.5 [13,22].

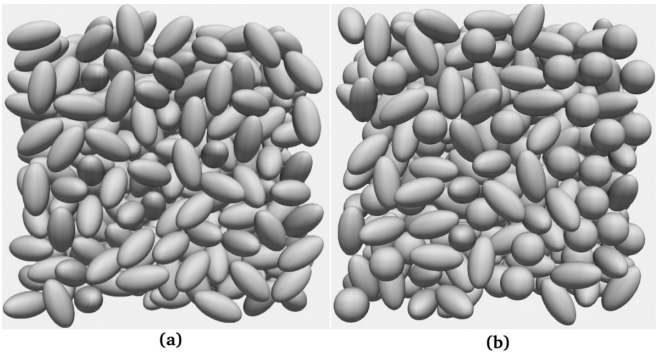

FIG. 11. (a) Snapshot of the monomeric prolate particle with $p = 2$ at $\phi = 0.5$ as obtained from the simulation. (b) The snapshot of the binary mixture of sphere and prolate $p = 2$ with the fraction of sphere $f^{1.0} = 0.40$. In both the systems we do not observe nematic transition.

To verify whether the nematic order is the only reason for the observed enhancement in the diffusion coefficient for the monomeric ER, we performed the simulation of a mixture of spheres and prolate particles at $p = 2$. Note that for $p = 2$ the isotropic-nematic transition is absent [59,60], which can also be observed in the snapshot shown in Fig. 11(a) for $\phi = 0.5$ and $f^{1.0} = 0$. We have plotted the transnational diffusion coefficient of only the prolate and sphere system in the mixture as a function of the total volume fraction ϕ in Fig. 12(a). The translational diffusion coefficient of $p = 2$ of the ellipsoids of one component crosses the corresponding sphere diffusion coefficient for $\phi > 0.35$. We have also confirmed that the nematic order is not observed in this case. This implies that the enhancement in diffusion coefficient happens due to the anisotropic shape of the particles, and the nematic phase just assists in the enhancement of the diffusion coefficient for the higher volume fractions.

In Fig. 12(b) we have plotted the rotational diffusion coefficient for the mixture at $f^{1.0} = 0.2$. Here we observe that due to the presence of spheres, for low ϕ the rotational diffusion coefficient is higher than the one-component prolate system. As the fraction of spheres increases, the prolate particle will have more free space for rotation, compared to the one-component prolate particle, at the same ϕ. When $\phi > 0.25$, we can observe that the rotational diffusion of all fractions agrees with the $f^{1.0} = 0$ case, as the crowding effect of the spheres increases indicating that the free space to perform rotational diffusion is equivalent to the one-component prolate case.

IV. DISCUSSION AND CONCLUSION

Recently, Roller *et al.* [13], showed the existence of liquid glass for monomeric ellipsoidal particles. To prevent the system from undergoing an isotropic nematic transition, the walls of the enclosed simulation box were made rough. They observed that the rotational diffusion tends towards zero without the nematic order. In the present paper, in the ellipsoid-sphere binary system with $f^{1.0} = 0.2$ we observe that the rotational diffusion coefficient tends towards the one-component case

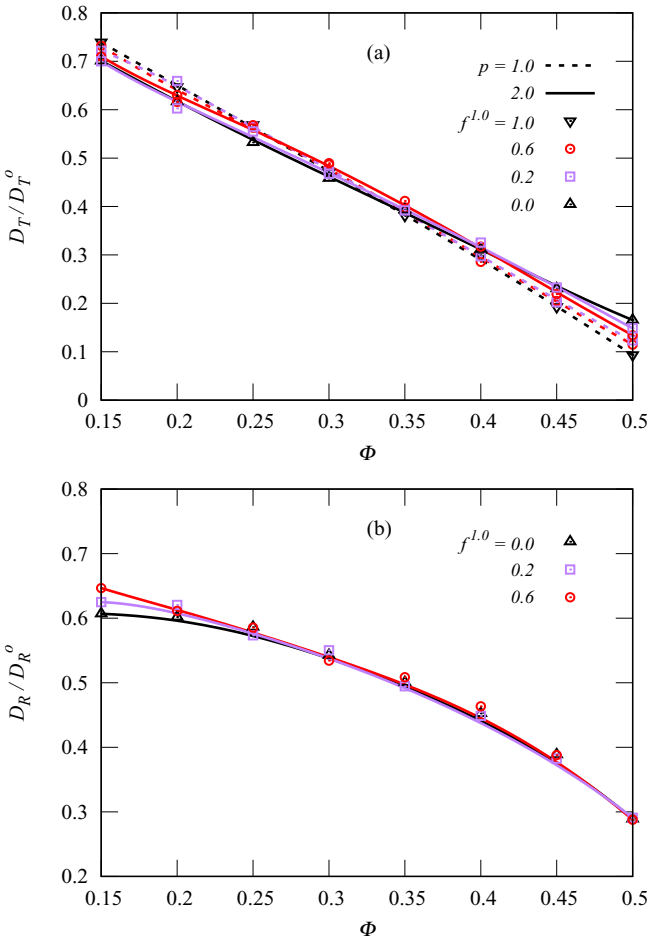

FIG. 12. (a) D_T^e/D_T^o shown for the spheres (dashed line) and prolate particle (solid line) with aspect ratio 2.0 at different ϕ in the binary mixture and the lines are guides to the eyes. The fraction of sphere in the system is as shown in the figure. (b) D_R^e/D_R^o is shown for the ellipsoidal particles $p = 2$ in the binary mixture with the fraction of the sphere as indicated in the figure. The solid line is a guide to the eye.

for $p = 4$ at $\phi = 0.5$. Note that in the one-component case the nematic transition happens for $\phi > 0.43$, while in the binary system we have shown that the nematic transition is absent, but still the rotational diffusion tends towards zero. Thus, adding polydispersity in the form of a sphere, we might be observing the liquid glass phase proposed by Roller *et al.* for the dynamics of the ellipsoidal particle in the binary mixture. When we further increase the fraction of sphere $f^{1.0} = 0.6$, the rotational diffusion is higher than the one-component case exhibiting only liquidlike behavior for the ellipsoidal particle.

As we increase the fraction of the sphere in the binary mixture, we observed that the nematic phase vanishes for the particular ϕ. Similar kinds of phase behavior have also been observed in the sphere-rod mixture [23] as well as for the prolate-sphere mixture [25]. Using the density functional theory, the same effect was observed by the authors of Ref. [26]. They also did not observe any demixing of the sphere and ellipsoidal systems similar to those observed in the present paper.

In the present paper, we were able to successfully extend the Brownian cluster dynamics method to include ellipsoids, which includes both prolate and oblate ellipsoidal particles. The ellipsoidal particle considered has a constant volume $\pi/6$, which is equivalent to a sphere of unit diameter. To identify the overlap between different ellipsoids, we employed the bounding box method where we enclose the ellipsoidal in a rectangular box if and only if the boxes overlap; we employ the ellipsoidal contact function to verify the ellipsoids overlap. If overlap is detected, we reject that particular movement step. The translational dynamics of ellipsoids is implemented by moving the center of mass of the ellipsoids in a random direction. The diffusions along the direction parallel to the symmetry axis and perpendicular to the symmetry axis are chosen according to Perrin's factor, which was solved for the stick boundary condition [47]. In order to mimic the rotational dynamics we employ the quaternion method to rotate the orientation vector along the long axis of the ER by using Perrin's factor for the rotation. In the present paper, one unit of time is defined as the time taken by a sphere of unit diameter and volume $\pi/6$ to travel its own diameter.

One of the drawbacks of the method is that the step size we choose should be smaller than the interparticle distance to define the diffusion properly. For a larger step size, we induce a lot of collision with the neighboring particle, thereby reducing the diffusion coefficient of the system. For a smaller step size, the physical time over which we can explore the system reduces. We have shown that the diffusion coefficient of the dilute system agrees with the analytical equation given by Perrin *et al.* [47], confirming our definition of time is correct. The isodiffusivity line for the ellipsoidal particle as a function of volume fraction was predicted to have a swallowlike shape by event-driven molecular dynamics, which agrees with our method as well. Although the absolute values of the diffusion coefficient do not match because of the way the diffusion is defined in both cases, except for the sphere where both methods yield the same result. We have also extended the BCD method to incorporate the binary ellipsoid and sphere systems. Here, we observe that even though the diffusion of a single sphere is faster than that of ellipsoids, the diffusion coefficient of ellipsoids is higher than that of the corresponding sphere at $p = 4$ and 2 for a larger volume fraction. It was also shown that the reason for the increase in the diffusion coefficient is due to the particle asymmetry, and the isotropic nematic transition only enhances the absolute value of the diffusion coefficient. In the binary mixture, we have shown that as the fraction of spheres increases, nematic ordering starts breaking in the region close to the sphere. It leads to a gradual decrease in the order parameter and finally to the isotropic phase, as shown in the phase diagram. We also calculated the diagram of the isotropic nematic phase, where we observed that as the fraction of spheres increases, ϕ also has to be increased to maintain the nematic phase. It will be interesting to study the nematic phases of a mixture of ellipsoids, where both particles undergo nematic transition for a range of fractions.

ACKNOWLEDGMENTS

We would like to acknowledge the IIT Delhi HPC facility for computational resources. V.A.V.

would like to acknowledge the UGC-CSIR funding agency for a fellowship. S.B.B. acknowledges partial support from DST-SERB India (Project No. CRG/2019/000580).

[1] J. Taffs and C. Patrick Royall, Nat. Commun. **7**, 13225 (2016).
[2] P. N. Pusey, E. Zaccarelli, C. Valeriani, E. Sanz, W. C. K. Poon, and M. E. Cates, Phil. Trans. R. Soc. A **367**, 4993 (2009).
[3] T. Sentjabrskaja, E. Zaccarelli, C. De Michele, F. Sciortino, P. Tartaglia, T. Voigtmann, S. U. Egelhaaf, and M. Laurati, Nat. Commun. **7**, 11133 (2016).
[4] S. Babu, M. Rottereau, T. Nicolai, J. C. Gimel, and D. Durand, Eur. Phys. J. E **19**, 203 (2006).
[5] S. O. Morgan, J. Fox, C. Lowe, A. M. Adawi, J. S. G. Bouillard, G. J. Stasiuk, T. S. Horozov, and D. M. A. Buzza, Phys. Rev. E **103**, 042604 (2021).
[6] E. Zaccarelli and W. C. K. Poon, Proc. Natl. Acad. Sci. USA **106**, 15203 (2009).
[7] S. Babu, J.-C. Gimel, and T. Nicolai, J. Chem. Phys. **130**, 064504 (2009).
[8] N. E. Valadez-Pérez, Y. Liu, and R. Castañeda-Priego, Phys. Rev. Lett. **120**, 248004 (2018).
[9] T. Hueckel, G. M. Hocky, and S. Sacanna, Nat. Rev. Mater. **6**, 1053 (2021).
[10] J. S. Myung, F. Roosen-Runge, R. G. Winkler, G. Gompper, P. Schurtenberger, and A. Stradner, J. Phys. Chem. B **122**, 12396 (2018).
[11] A. Pal, V. A. Martinez, H. Ito Thiago, A. Jochen, J. Crassous Jérôme, K. Poon Wilson C., and P. Schurtenberger, Sci. Adv. **6**, eaaw9733 (2021).
[12] K. V. Edmond, M. T. Elsesser, G. L. Hunter, D. J. Pine, and E. R. Weeks, Proc. Natl. Acad. Sci. USA **109**, 17891 (2012).
[13] J. Roller, A. Laganapan, J.-M. Meijer, M. Fuchs, and A. Zumbusch, Proc. Natl. Acad. Sci. USA **118**, e2018072118 (2021).
[14] A. Cuetos and A. Patti, Phys. Rev. E **101**, 052702 (2020).
[15] W. S. Xu, Y. W. Li, Z. Y. Sun, and L. J. An, J. Chem. Phys. **139**, 024501 (2013).
[16] Z. Zheng, R. Ni, Y. Wang, and Y. Han, Sci. Adv. **7**, eabd1958 (2021).
[17] S. Davatolhagh and S. Foroozan, Phys. Rev. E **85**, 061707 (2012).
[18] Y. Peng, L. Lai, Y.-S. Tai, K. Zhang, X. Xu, and X. Cheng, Phys. Rev. Lett. **116**, 068303 (2016).
[19] A. Stradner and P. Schurtenberger, Soft Matter **16**, 307 (2020).
[20] Y. Han, A. M. Alsayed, M. Nobili, J. Zhang, T. C. Lubensky, and A. G. Yodh, Science **314**, 626 (2006).
[21] C. De Michele, A. Scala, R. Schilling, and F. Sciortino, J. Chem. Phys. **124**, 104509 (2006).
[22] M. Letz, R. Schilling, and A. Latz, Phys. Rev. E **62**, 5173 (2000).
[23] D. Antypov and D. J. Cleaver, Chem. Phys. Lett. **377**, 311 (2003).
[24] R. Aliabadi, M. Moradi, and S. Varga, J. Chem. Phys. **144**, 074902 (2016).
[25] C. E. Alavrez and M. Mazars, arXiv:1405.2357.
[26] A. Samborski and G. T. Evans, J. Chem. Phys. **101**, 6005 (1994).
[27] A. Das and D. T. Limmer, J. Chem. Phys. **154**, 014107 (2021).
[28] C. De Michele, R. Schilling, and F. Sciortino, Phys. Rev. Lett. **98**, 265702 (2007).
[29] P. Bereolos, J. Talbot, M. P. Allen, and G. T. Evans, J. Chem. Phys. **99**, 6087 (1993).
[30] N. Kern and D. Frenkel, J. Chem. Phys. **118**, 9882 (2003).
[31] D. Frenkel and B. M. Mulder, Mol. Phys. **55**, 1171 (1985).
[32] D. Frenkel, B. M. Mulder, and J. P. McTague, Phys. Rev. Lett. **52**, 287 (1984).
[33] X. Sun, T. Lin, and J. D. Gezelter, J. Chem. Phys. **128**, 234107 (2008).
[34] S. Babu, J.-C. Gimel, T. Nicolai, and C. De Michele, J. Chem. Phys. **128**, 204504 (2008).
[35] S. Babu, J. C. Gimel, and T. Nicolai, Eur. Phys. J. E **27**, 297 (2008).
[36] J. C. Gimel, D. Durand, and T. Nicolai, Phys. Rev. B **51**, 11348 (1995).
[37] J. C. Gimel, T. Nicolai, and D. Durand, J. Sol-Gel Sci. Technol. **15**, 129 (1999).
[38] M. Rottereau, J. C. Gimel, T. Nicolai, and D. Durand, Eur. Phys. J. E **15**, 133 (2004).
[39] M. Rottereau, J. C. Gimel, T. Nicolai, and D. Durand, Eur. Phys. J. E **15**, 141 (2004).
[40] S. Babu, J. C. Gimel, and T. Nicolai, J. Chem. Phys. **127**, 054503 (2007).
[41] Z. Shireen and S. B. Babu, J. Chem. Phys. **147**, 054904 (2017).
[42] Z. Shireen and S. B. Babu, Soft Matter **14**, 9271 (2018).
[43] A. Prabhu, S. B. Babu, J. S. Dolado, and J.-C. Gimel, J. Chem. Phys. **141**, 024904 (2014).
[44] I. Malhotra and S. B. Babu, Pure Appl. Chem. **90**, 1085 (2018).
[45] I. Malhotra and S. B. Babu, J. Chem. Phys. **151**, 084901 (2019).
[46] I. Malhotra and S. B. Babu, J. Phys.: Condens. Matter **32**, 355101 (2020).
[47] F. Perrin, J. Phys. Radium **5**, 497 (1934).
[48] W. Dzwinel, J. Kitowski, and J. Mościński, Mol. Simul. **7**, 171 (1991).
[49] C. De Michele, J. Comput. Phys. **229**, 3276 (2010).
[50] J. W. Perram and M. Wertheim, J. Comput. Phys. **58**, 409 (1985).
[51] D. ben Avraham and S. Havlin, *Diffusion and Reactions in Fractals and Disordered Systems* (Cambridge University, Cambridge, England, 2000).
[52] J. K. G. Dhont, in *Studies in Interface Science* (Elsevier, Amsterdam, 1996), Vol. 2, p. 69.
[53] R. Vasanthi, S. Bhattacharyya, and B. Bagchi, J. Chem. Phys. **116**, 1092 (2002).
[54] Z. Zheng and Y. Han, J. Chem. Phys. **133**, 124509 (2010).
[55] J. Happel and H. Brenner, *Low Reynolds Number Hydrodynamics with Special Applications to Particulate Media*, 1st ed. (Springer, New York, 1983).
[56] S. Tang, G. T. Evans, C. P. Mason, and M. P. Allen, J. Chem. Phys. **102**, 3794 (1995).

[57] B. Van Roie, J. Leys, K. Denolf, C. Glorieux, G. Pitsi, and J. Thoen, Phys. Rev. E **72**, 041702 (2005).
[58] R. Eppenga and D. Frenkel, Mol. Phys. **52**, 1303 (1984).
[59] G. Odriozola, J. Chem. Phys. **136**, 134505 (2012).
[60] G. Bautista-Carbajal, A. Moncho-Jordá, and G. Odriozola, J. Chem. Phys. **138**, 064501 (2013).
[61] M. P. Allen, Phys. Rev. Lett. **65**, 2881 (1990).